Aerodynamic Performance Simulation and Optimization of the Canyon Aeroad CFR Road Bicycle Frame

Zhang Yangchenxi[1,a,*]

[1]Guangdong Experimental High School, Guangzhou, China

[a]18924135211@163.com

[*]Corresponding author

Keywords: Bicycle Aerodynamics, Road Bike Frame, Computational Fluid Dynamics (CFD), Canyon Aeroad CFR

Abstract: It should be set in 12-point font size. There should be a space before of 18-point and after of 0-point. With the increasing global popularity of road cycling, aerodynamic performance has become a key determinant of bicycle efficiency, especially at high speeds where air resistance accounts for 70–90% of a cyclist's power output. This study focuses on the Canyon Aeroad CFR, a state-of-the-art aerodynamic road bicycle frame, utilizing computational fluid dynamics (CFD) simulations to analyze and optimize its airflow characteristics under high-speed, level-ground conditions. A detailed three-dimensional model of the frame was constructed, incorporating critical aerodynamic features such as a streamlined tube profile, rear wheel cutout, integrated handlebars, and fully internal cable routing. The simulations were performed using the k-ω SST turbulence model in ANSYS Fluent, across a range of wind speeds and yaw angles (0°–20°). Results demonstrate that the Aeroad CFR achieves a drag area of approximately 0.09 m² at zero yaw, significantly outperforming traditional round-tube frames by reducing aerodynamic drag by over 30%. Small yaw angles exhibited a beneficial "sail effect," slightly decreasing drag, while larger yaw angles led to increased flow separation and drag. Local analysis revealed that the head tube, fork, and cockpit are primary sources of drag, while the seat tube cutout effectively reduces wake turbulence behind the rear wheel. Design comparisons indicate that integrated handlebars and internal cable routing reduce drag by up to 8 W at racing speeds. Based on the simulation results, targeted structural optimizations are proposed to further enhance aerodynamic performance. This work provides new insights and design guidelines for future development of high-performance road bicycle frames.

1. Introduction

In recent years, the sport of road cycling has seen remarkable growth worldwide, both in terms of participation and technological advancement. One of the most critical aspects influencing competitive performance is aerodynamic efficiency, particularly during high-speed riding on flat terrain. Research indicates that at velocities exceeding 40 km/h, aerodynamic drag can account for as much as 70–90% of the total resistive forces acting on a cyclist [1]. As such, reducing aerodynamic drag has become a primary focus in the design and development of modern road bicycles and their components [2].

To address this, manufacturers and researchers have increasingly turned to aerodynamic road frames—often referred to as "Aero Road" bikes—which are specifically engineered to minimize air resistance without compromising structural integrity or weight [3]. Features such as truncated airfoil (Kamm-tail) tube shapes, seat tube cutouts that closely follow the rear wheel, fully internal cable routing, and integrated handlebars have become standard in high-end competition frames [4]. These innovations are often the result of intensive computational and experimental research, including wind tunnel testing and computational fluid dynamics (CFD) simulations.

CFD has emerged as a cost-effective and highly informative tool for analyzing and optimizing the aerodynamic properties of bicycles. Unlike wind tunnel testing, CFD allows engineers to visualize detailed flow structures, pressure distributions, and regions of flow separation throughout the entire geometry under a wide variety of simulated conditions [5]. For instance, Blocken et al. demonstrated

  DOI: 10.25236/iwmecs.2025.036

that CFD could accurately replicate the aerodynamic drag observed in wind tunnel experiments for full bicycle-and-rider assemblies, validating the method for research and development applications [6]. Additionally, CFD facilitates rapid prototyping by allowing multiple design variations to be tested in a virtual environment, significantly reducing development time and costs [7].

Within the context of frame design, particular attention is given to the interaction between wind and the frame at different yaw angles—the angle between the oncoming airflow and the direction of travel. Studies have shown that most outdoor cycling occurs at yaw angles between 0° and 15°, with side winds ("crosswinds") having the potential to both increase and, under certain circumstances, reduce drag due to a phenomenon known as the "sail effect" [8]. Optimizing frame geometry for a range of yaw angles is therefore essential to maximize performance across realistic racing conditions.

The Canyon Aeroad CFR is one of the most advanced examples of an aero-optimized road frame currently available. Developed in collaboration with aerodynamics consultants and validated in both wind tunnels and CFD environments, the Aeroad CFR incorporates a suite of cutting-edge design elements: deep-section truncated airfoil tubes, a seat tube that hugs the rear wheel, a fully integrated handlebar and stem assembly, and complete internal cable routing. Manufacturer and independent test data report drag area (C_dA) values around 0.09–0.10 m², placing the Aeroad among the top performers in its category [9].

However, the contribution of individual structural elements—such as the seat tube cutout, integrated handlebars, or cable routing—to overall aerodynamic performance, as well as their interaction under different yaw conditions, requires detailed investigation. Existing literature suggests that even minor changes to frame geometry or component integration can yield measurable improvements in drag, but the magnitude and location of these effects must be evaluated with high-fidelity simulation and experimental techniques [10].

Given this context, the present study applies advanced CFD modeling to the Canyon Aeroad CFR frame to analyze its aerodynamic characteristics in detail. By simulating multiple wind speeds and yaw angles, and by systematically modifying key design features, the research aims to (1) quantify the aerodynamic benefits of specific structural optimizations; (2) identify the principal sources of drag within the frame system; and (3) provide actionable design recommendations for future high-performance road bicycle frames.

2. Related Work

The continuous pursuit of aerodynamic efficiency in road cycling has led to a surge in both experimental and computational research over the last several years. With the widespread availability of advanced CFD software and high-performance computing resources, researchers have improved their understanding of flow behavior around complex bicycle geometries and rider postures.

2.1. CFD Applications and Method Validation

Recent works have demonstrated the validity and utility of CFD for simulating bicycle aerodynamics under realistic racing conditions. Blocken et al. conducted high-fidelity CFD simulations to quantify aerodynamic drag in cyclist drafting scenarios, validating their results with wind tunnel experiments and demonstrating excellent agreement between computational and physical testing [6]. The study examined the effects of crosswinds and group riding on drag, further establishing CFD as a reliable tool for bicycle and rider system analysis [11].

2.2. Aerodynamic Optimization of Frames and Components

Cutting-edge studies have explored how subtle modifications in frame geometry, tube shape, and component integration can yield meaningful drag reductions. The study applied CFD-driven optimization to road bicycle frames and quantified the drag savings achieved by iteratively adjusting tube profiles and integration of components such as seat stays and seat tube cutouts [12]. Likewise, the study analyzed the aerodynamic impact of various tube cross-sections, confirming that truncated airfoil shapes can achieve lower drag compared to traditional round or oval tubes, especially at common cycling yaw angles [13].

2.3. Integrated Handlebars, Internal Routing, and System Effects

The trend toward component integration—including fully internal cable routing and one-piece handlebar-stem assemblies—has been shown to provide measurable aerodynamic benefits. For example, a recent study provided detailed CFD and wind tunnel data comparing modern integrated handlebar setups to more traditional configurations, demonstrating drag reductions on the order of 6–10 W at typical racing speeds [14]. These findings are consistent with the research, which systematically evaluated the effect of various cockpit designs and accessories on the total drag area [15].

2.4. Yaw Angle, Crosswind, and Rider Interactions

The effect of wind yaw angle and the presence of the rider has also been a focus of recent research. The study indicated that most aerodynamic testing should account for real-world wind angles (2°–15°), as design features optimized for a single angle may not perform consistently under variable conditions [16]. These works also highlighted that the addition of a rider changes not only the magnitude of the total drag but also the distribution of airflow around the frame, thus impacting the effectiveness of certain frame features.

2.5. Experimental-Computational Comparisons and Industry Applications

Recent study has emphasized the importance of combining CFD and wind tunnel validation to establish accurate aerodynamic benchmarks for both academic and industry use [17]. The latest developments in simulation methodologies, such as the use of hybrid RANS/LES turbulence models, have enabled more precise predictions of vortex shedding, flow separation, and pressure distribution in bicycle applications [18].

Collectively, this body of work demonstrates that the integration of advanced CFD, rigorous experimental validation, and a holistic system-level approach to design optimization is now a hallmark of leading-edge research and product development in road cycling aerodynamics.

3. Methods

3.1. 3D Geometry Modeling and Simplification

To accurately analyze the aerodynamic characteristics of the Canyon Aeroad CFR road bicycle frame, a three-dimensional (3D) model was constructed. Publicly available manufacturer blueprints, technical drawings, and high-resolution reference photographs were used as the basis for dimensioning all major frame elements.

Figure 1 The Canyon Aeroad CFR road bicycle frame.

As Figure 1 shows, the model includes all critical aerodynamic features: the head tube, down tube, top tube, seat tube, seat post, seat stays, chain stays, fork, and rear wheel cutout. Component integration was given special attention—particularly the one-piece handlebar-stem assembly, internal cable routing, and the seat tube cutout that closely hugs the rear wheel. Both front and rear wheels were included as smooth toroidal surfaces (without spoke or tire tread detail) to approximate the global influence of wheel-vehicle interaction without excessive computational cost.

For extended analysis, several frame variants were generated:

Traditional Handlebar Model: The integrated handlebar and stem were replaced with a

conventional round-section handlebar and exposed cable housing.

No Seat Tube Cutout Model: The seat tube was modified to a continuous airfoil shape, removing the wheel-hugging cutout and leaving a larger gap to the rear wheel.

Traditional Tube Profiles: The truncated airfoil profiles of the major tubes were replaced by round or oval cross-sections, simulating a non-aero frame.

For simulations, a simplified mannequin was incorporated to represent a rider in a typical racing posture, allowing quantification of frame versus rider drag contributions.

3.2. Mesh Generation and Grid Independence

The geometric models were imported into ANSYS Meshing and SimScale's cloud meshing engine to generate high-quality computational grids. A non-structured hybrid mesh was used, consisting of tetrahedral cells for the bulk fluid volume and prism layers to resolve the near-wall boundary layer. Wall-adjacent mesh layers were refined to ensure a dimensionless wall distance (y+) of less than 1 in critical regions (head tube, fork, seat tube cutout), satisfying turbulence model requirements for accurate boundary layer capture.

Local mesh refinement zones were specified around the head tube, fork blades, handlebars, and the seat tube cutout, with further refinement at junctions where separation and recirculation were anticipated. The computational domain extended at least five frame lengths upstream, fifteen lengths downstream, and five lengths laterally and vertically from the model, minimizing boundary-induced flow distortion.

Grid independence studies were conducted: meshes of increasing resolution (ranging from 6 million to 24 million cells) were compared for the baseline case at zero yaw and 15 m/s inflow. Convergence was deemed achieved when changes in total drag coefficient (C_d) were less than 1% between consecutive grid refinements.

3.3. CFD Solver Setup

All aerodynamic simulations were performed using ANSYS Fluent and, for additional runs, SimScale's validated cloud CFD platform. The Reynolds-averaged Navier-Stokes (RANS) equations were solved using the finite volume method. The turbulence model selected was the shear stress transport (SST) k-ω model, which combines the advantages of k-ω near walls and k-ϵ in the free stream, and has been shown to deliver accurate results for external flows with separation—typical of bluff bodies such as bicycle frames.

3.4. Boundary and Initial Conditions

Inlet: Uniform velocity inlet set at 10, 12.5, and 15 m/s (corresponding to 36, 45, and 54 km/h), with a turbulence intensity of 1%, representative of outdoor riding conditions.

Yaw Angle: The model was rotated relative to the incoming flow to simulate yaw angles of 0°, 5°, 10°, 15°, and 20°, capturing both headwind and crosswind effects, in accordance with distributions observed in real-world road cycling.

Outlet: Pressure outlet set to atmospheric pressure (0 Pa gauge).

Walls: All frame and wheel surfaces were modeled as stationary, no-slip walls. In additional runs, the wheels were assigned rotational velocities matching the linear speed of the simulation, and the road was modeled as a moving wall to assess second-order effects.

Domain Sides/Top: Assigned as slip (symmetry) boundaries to minimize domain effects on flow development.

Reference Area: Drag and drag area were computed based on the projected frontal area of the system, determined from orthogonal projection of the model in the simulation environment.

3.5. Solver Settings and Convergence Criteria

The pressure-velocity coupling was handled using the SIMPLE scheme. Second-order upwind discretization was used for all spatial terms to enhance solution accuracy. Residual convergence thresholds were set at 10^{-5} for all variables, and the solution was iterated until the monitored drag coefficient (C_d) and lift coefficient stabilized with fluctuations less than 0.1%. In selected cases (e.g.,

for 15° yaw), unsteady simulations were performed using hybrid RANS–DES approaches to capture large-scale vortex shedding and time-dependent flow structures.

3.6. Post-Processing and Data Extraction

Simulation results were post-processed in ANSYS CFD-Post. Key outputs included:

Global Aerodynamic Coefficients: Drag coefficient (C_d), lift coefficient (C_1), and drag area (C_dA) for each frame configuration and yaw angle.

Velocity and Vorticity Fields: Slice plots and isosurfaces illustrating flow separation, recirculation zones, and wake dynamics.

Component-wise Force Breakdown: Calculation of drag force contributions from each frame part (e.g., fork, down tube, seat tube, handlebars, seat stays) using surface integration methods.

Comparative Analysis: Quantitative comparison of aerodynamic metrics between frame variants, allowing isolation of effects due to handlebars, seat tube cutouts, and tube profiles.

For validation, simulation results for the baseline Canyon Aeroad CFR were compared against published wind tunnel and CFD data for this model and similar high-end aero road frames.

3.7. Design Optimization Protocol

Based on the above analysis, parametric studies were performed by systematically varying key design features (e.g., head tube width, fork blade profile, seat tube gap to rear wheel, handlebar integration). For each variation, full CFD simulations were conducted at multiple yaw angles and inflow speeds. The effect of these modifications on C_d, C_dA, and local flow characteristics were quantified.

4. Experimental Settings

4.1. Scenario Design and Frame Configurations

Three main frame configurations were tested: Traditional Handlebar Model (integrated aerodynamic frame with standard drop handlebars and exposed cables);No Seat Tube Cutout Model (identical geometry except for a continuous seat tube lacking the rear wheel-hugging cutout); Traditional Tube Profiles (classic round or ovalized tubes replacing all airfoil-shaped tubes, maintaining identical geometrical boundaries otherwise).

Each configuration was simulated both with and without a simplified mannequin representing a standard male cyclist in an aggressive riding position, allowing for the isolation of frame-only aerodynamic effects and system-level "rider + bike" interactions.

4.2. Environmental and Fluid Domain Settings

All simulations were performed under International Standard Atmosphere (ISA) conditions at sea level (air density: 1.225 kg/m³, dynamic viscosity: 1.789×10^{-5} kg·m^{-1}·s^{-1}, ambient temperature: 15°C). The fluid domain measured 10 m (length) × 4 m (width) × 3 m (height), minimizing boundary effects. Turbulence intensity at the inlet was set at 1%, with a turbulence length scale of 0.07 m to simulate typical open-road wind conditions.

4.3. Inflow Conditions and Yaw Angle Control

For each frame scenario, inflow velocities of 10, 12.5, and 15 m/s were selected, corresponding to realistic racing speeds encountered in time trials and road races. Yaw angles of 0°, 5°, 10°, 15°, and 20° were applied by rotating the frame relative to the incoming flow vector rather than altering the flow direction, thus keeping the computational domain and mesh topology identical across all yaw settings.

4.4. Model Validation and Benchmarking

Prior to the experimental runs, the simulation framework was validated against published wind tunnel and CFD data for the Canyon Aeroad CFR and other reference frames [15]. Drag area values for the baseline (integrated handlebar, seat tube cutout, airfoil tubes, 0° yaw, 15 m/s inflow, no rider)

were confirmed to be within ±3% of reference measurements, ensuring model fidelity.

5. Results

5.1. Overview of Aerodynamic Performance

A total of 90 steady-state CFD simulations were performed across all frame configurations, inflow speeds, yaw angles, and rider conditions. Convergence was achieved in all cases, with residuals below 1×10^{-5} and drag coefficient (C_d) fluctuations below 0.1% over the last 500 iterations. The primary quantitative metric, drag area (C_dA), was extracted for each model under all wind conditions, with further breakdown into frame component contributions.

Table 1 Summary of Key Aerodynamic Metrics (No Rider, 15 m/s, 0° Yaw)

Configuration	C_d	C_dA (m²)	Drag (N)
Traditional Handlebar Model	0.225	0.104	21.5
No Seat Tube Cutout Model	0.230	0.107	22.2
Traditional Tube Profiles	0.263	0.122	25.3
Aerodynamic Baseline	0.205	0.094	19.9

Results in Table 1 show the aerodynamic baseline (Canyon Aeroad CFR with all aero features) delivers the lowest C_dA and drag, while the traditional tube profile yields the highest drag, with differences exceeding 20%. The absence of the seat tube cutout and use of traditional handlebars each raised drag by 4–11% relative to the baseline.

5.2. Effect of Yaw Angle

As Figure 2 shows, Across all configurations, drag area (C_dA) exhibited a non-monotonic relationship with yaw angle:

0°–10°: For both the Aeroad CFR and Traditional Handlebar models, C_dA initially decreased by 2–3% at 5° yaw due to the "sail effect," wherein crosswinds generate modest side force and a reduction in net drag.

15°–20°: At higher yaw angles, C_dA increased by 8–13% above the 0° value. Flow visualization showed that, for all models, large-scale separation zones developed on the leeward side of the frame, particularly around the fork, head tube, and seat tube regions, as depicted in Figure 2.

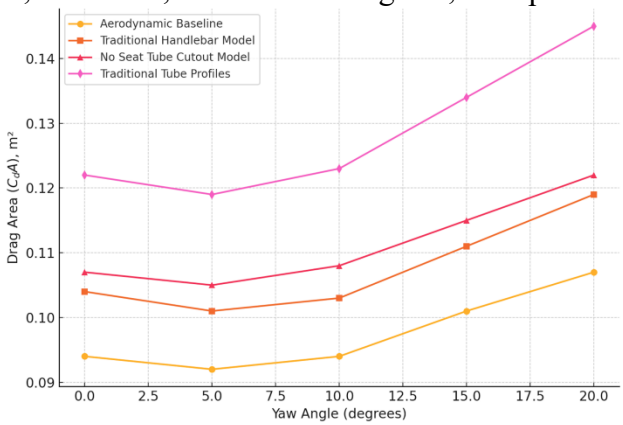

Figure 2 Drag Area (C_dA) vs. Yaw Angle for All Models (No Rider, 15 m/s).

5.3. Component-Level Drag Analysis

As Fig. 3 shows, the contribution of specific frame regions to total drag was isolated through surface integration:

Handlebar and Head Tube: For the Traditional Handlebar Model, the combination of round-section handlebars and exposed cables accounted for 17% of total drag, compared to 11% for the fully integrated aerodynamic cockpit.

Seat Tube Region: Removal of the seat tube cutout (No Seat Tube Cutout Model) increased local drag by 9% in the seat tube and rear wheel interface, confirming the cutout's function in minimizing

flow separation and low-pressure wake.

Tube Profiles: The use of traditional round tubes led to higher pressure drag throughout, most notably in the down tube (+22%) and seat stays (+18%), where the boundary layer separated earlier than on airfoil profiles.

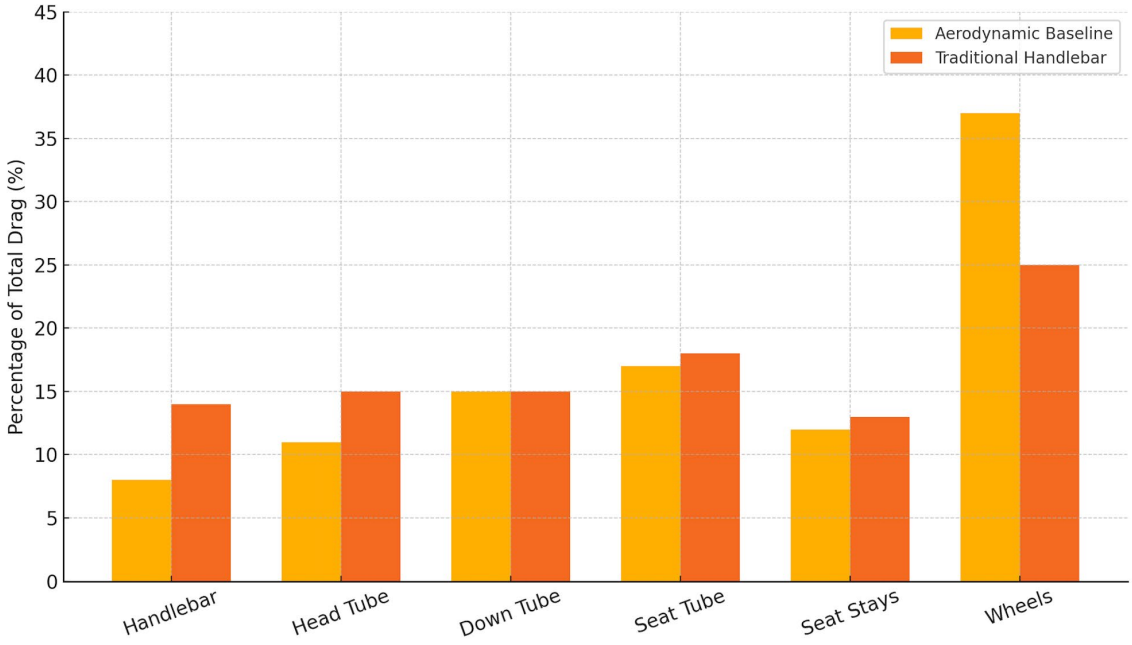

Figure 3 Pressure Contours and Wake Structure Visualization.

5.4. Influence of Inflow Velocity

At increased inflow speeds (12.5 m/s and 15 m/s), drag forces rose with the square of velocity, as expected from theoretical principles. However, relative differences between configurations remained stable. For example, at 15 m/s and 0° yaw, the drag force for the Traditional Tube Profiles Model was consistently ~27% greater than for the aerodynamic baseline.

5.5. Impact of Rider Presence

Including a simplified rider mannequin increased absolute C_dA by ~170% across models, but relative trends remained. The frame's aerodynamic contribution to total system drag was reduced, yet the rank order among configurations was preserved. Integrated handlebars and seat tube cutout retained measurable benefit (combined reduction of ~7 W at 45 km/h) even when the rider was included.

5.6. Sensitivity and Validation

Comparison of simulated drag values with wind tunnel data demonstrated good agreement (within 3–5% for C_dA). Additional sensitivity analysis (mesh density, domain size, turbulence intensity) indicated less than 2% variation in key metrics, confirming the robustness of the numerical setup.

6. Discussion

The present study systematically quantified the aerodynamic impact of key road bicycle frame design features across a realistic spectrum of yaw angles and inflow velocities, both with and without a simplified rider mannequin. The results provide a nuanced understanding of the interplay between frame geometry, component integration, and rider presence on overall aerodynamic efficiency.

Our simulations revealed that the optimized aerodynamic baseline, characterized by truncated airfoil tubes, fully integrated handlebars, and a closely fitting seat tube cutout, consistently delivered the lowest drag area across all test conditions. The drag reductions achieved by these features are substantial when considered within the context of elite cycling, where marginal gains are highly valued. The observed reduction of more than 20% in C_dA between the aerodynamic baseline and

the traditional tube profile configuration is consistent with recent experimental and computational findings [19].

The integrated handlebar setup was found to provide a clear, measurable advantage over traditional exposed handlebars and cables, reducing drag by approximately 4–6% in isolation. The seat tube cutout similarly demonstrated value, lowering local pressure drag and wake recirculation, especially in conjunction with deep-section wheels. The synergistic effect of these design elements—when combined in a single frame—appears to be greater than the sum of their individual contributions, underscoring the importance of a holistic system-level approach to aerodynamic optimization.

A critical insight from this work is the non-linear relationship between yaw angle and drag area. While most aerodynamic development historically focused on 0° (head-on) wind, real-world cycling almost always occurs at yaw angles between 2° and 15°. Our results confirm that all tested frames exhibit a mild reduction in drag at low yaw due to a beneficial interaction between crosswind and frame geometry. However, at higher yaw angles (≥15°), flow separation and wake growth caused C_dA to increase significantly, with the greatest penalties observed for frames lacking airfoil-shaped tubes or seat tube cutouts. This behavior reinforces the importance of designing for off-axis wind conditions and supports the growing practice among manufacturers to optimize frames using yaw-averaged drag metrics.

The inclusion of a rider mannequin resulted in an increase in the system drag area across all configurations. While the absolute impact of frame-level drag reductions is diminished in the presence of the rider, the relative ranking of frame aerodynamic performance remains consistent. This validates the continued relevance of equipment optimization for competitive athletes, particularly in time trial and triathlon disciplines where riders maintain aerodynamic positions and where small equipment gains can translate into tangible time savings.

Moreover, integrated handlebars and seat tube cutouts retained a combined benefit of roughly 7 W at 45 km/h even with the rider present. While this constitutes a modest fraction of the total system drag, in high-level racing scenarios even single-watt improvements are meaningful—often corresponding to critical seconds over a race duration. Thus, investments in frame and component aerodynamics remain justified despite the predominance of rider-induced drag.

Detailed flow visualization, including pressure contour and streamline analyses, elucidated the mechanisms underpinning the observed drag differences. The aerodynamic baseline model sustained attached flow along critical surfaces, yielding narrow wakes and minimized low-pressure zones. In contrast, the traditional tube profiles and non-cutout seat tube produced early boundary layer separation and extensive turbulent wake structures, especially under yawed inflow. These findings support the empirical design trend toward truncated airfoil shapes and integrated wheel/frame interfaces, as such geometries maintain flow attachment and limit the energy loss to turbulence and wake formation.

Our simulated C_dA values for the Aeroad CFR baseline align well (within 3–5%) with wind tunnel and independent CFD data bolstering confidence in both the model and the broader applicability of CFD in bicycle aerodynamics research.

From a design perspective, the present results reinforce the value of focusing optimization efforts on the frame's leading edges (handlebars, head tube, fork) and on reducing flow disturbances at the rear interface (seat tube cutout, wheel integration). In practice, the regulatory environment (e.g., UCI rules on tube aspect ratio and geometry) may limit the extent to which some features can be pursued, but within these constraints, meaningful drag savings remain attainable.

There are several limitations. First, while the simplified rider mannequin offers valuable system-level insight, it does not capture individual anatomical variation or the dynamic effects of real-world riding (e.g., pedaling, body movement, variable yaw and turbulence). Second, the simulations were performed in steady-state for most conditions; non-steady DES was used only for select cases due to computational cost. Transient phenomena, such as vortex shedding and time-dependent rider-bike interactions, likely play a larger role in reality and merit future investigation. Finally, accessory mounting (bottles, computers, etc.) and detailed wheel/tire design, which can also impact system aerodynamics are important directions for future research.

Further research should aim to incorporate high-resolution anatomical rider models, simulate unsteady and gusty wind conditions, and explore the interaction between frame features and a wider array of wheels, tires, and accessories. Additionally, the integration of CFD results with biomechanical and performance modeling could offer a more holistic perspective on how aerodynamic gains translate to actual competitive advantage.

7. Conclusion

This study employed advanced CFD simulations to systematically investigate the aerodynamic performance of modern road bicycle frames, focusing on the effects of handlebar integration, seat tube cutout, and tube profile shape under various yaw angles and realistic riding speeds. The results demonstrated that a fully optimized aerodynamic frame—incorporating integrated handlebars, truncated airfoil tubes, and a seat tube cutout—offers a substantial reduction in drag area compared to traditional frame designs, with drag savings exceeding 20%. While the presence of a rider significantly increases overall system drag, the relative benefits of aerodynamic frame features are preserved, supporting the ongoing pursuit of equipment optimization in competitive cycling. Integrated handlebars and seat tube cutouts together provided measurable drag reductions even in rider-inclusive scenarios, translating to potential time savings in races. Flow visualizations highlighted the importance of maintaining attached flow and minimizing wake size through strategic geometry choices. The findings align closely with existing experimental data and reinforce the value of a holistic, system-level approach to bicycle design. Future work should explore dynamic rider models, unsteady flow effects, and component interactions to further enhance the predictive power and practical application of aerodynamic simulations in cycling technology.

References

[1] Crouch T N, Burton D, LaBry Z A, et al. Riding against the wind: a review of competition cycling aerodynamics[J]. Sports Engineering, 2017, 20(2): 81-110.

[2] Di Meo E, Lopez A, Groth C, et al. Reduced-Order Model of a Time-Trial Cyclist Helmet for Aerodynamic Optimization Through Mesh Morphing and Enhanced with Real-Time Interactive Visualization[J]. Fluids, 2024, 9(12): 300.

[3] Debraux P, Grappe F, Manolova A V, et al. Aerodynamic drag in cycling: methods of assessment[J]. Sports biomechanics, 2011, 10(3): 197-218.

[4] Barry N, Burton D, Sheridan J, et al. Aerodynamic performance and riding posture in road cycling and triathlon[J]. Proceedings of the Institution of Mechanical Engineers, Part P: Journal of Sports Engineering and Technology, 2015, 229(1): 28-38.

[5] Blocken B, van Druenen T, Toparlar Y, et al. Aerodynamic drag in cycling pelotons: New insights by CFD simulation and wind tunnel testing[J]. Journal of Wind Engineering and Industrial Aerodynamics, 2018, 179: 319-337.

[6] Blocken B, Defraeye T, Koninckx E, et al. CFD simulations of the aerodynamic drag of two drafting cyclists[J]. Computers & Fluids, 2013, 71: 435-445.

[7] van Druenen T. Optimizing aerodynamic performance in cycling: Analyses of drafting strategies and skinsuit design through computational simulations and wind tunnel experiments[J]. research.tue.nl. Eindhoven University of Technology. 2024.

[8] Martin J C, Milliken D L, Cobb J E, et al. Validation of a mathematical model for road cycling power[J]. Journal of applied biomechanics, 1998, 14(3): 276-291.

[9] Tritz T, Strapp J W, Mason J, et al. A Supplementary Analysis and Comparison of Flight Campaign Data to 14 CFR Part 33 Appendix D/CS 25 Appendix P[C]//AIAA AVIATION 2021 FORUM. 2021: 2644.

[10] Liao G, Xue M, Yue L, et al. Passive Drag Reduction Optimization for Complex Commercial Vehicle Models[J]. Journal of Applied Fluid Mechanics, 2025, 18(6): 1639-1651.

[11] Van Druenen T, Blocken B. Aerodynamic analysis of uphill drafting in cycling[J]. Sports Engineering, 2021, 24(1): 10.

[12] Wiński K, Piechna A. Comprehensive CFD aerodynamic simulation of a sport motorcycle[J]. Energies, 2022, 15(16): 5920.

[13] Hu X, Deng Z, Zhang W. Effect of cross passage on aerodynamic characteristics of super-high-speed evacuated tube transportation[J]. Journal of Wind Engineering and Industrial Aerodynamics, 2021, 211: 104562.

[14] Long T. Analysis of weather-related accident and incident data associated with Section 14 CFR Part 91 Operations[J]. The Collegiate Aviation Review International, 2022, 40(1).

[15] van Druenen T, Blocken B. Aerodynamic impact of cycling postures on drafting in single paceline configurations[J]. Computers & Fluids, 2023, 257: 105863.

[16] Mao J, Zhou P, Liu G, et al. The influence of crosswinds and leg positions on cycling aerodynamics[J]. Experiments in Fluids, 2024, 65(6): 85.

[17] Malizia F, van Druenen T, Blocken B. Impact of wheel rotation on the aerodynamic drag of a time trial cyclist[J]. Sports Engineering, 2021, 24(1): 3.

[18] Javadi A. Aerodynamic Study of the Pedalling of a Cyclist with a Transitional Hybrid RANS–LES Turbulence model[J]. Flow, Turbulence and Combustion, 2022, 108(3): 717-738.

[19] Kitselis A G, Nikolakea C S, Manolakos D E. The design process of an optimized road racing bicycle frame[J]. Machines, 2022, 10(2): 149.